KHAN, A. A. & BAUR, W. H. (1973). *Acta Cryst.* B**29**, 2721–2726.
KOBAYASHI, J. & UESU, Y. (1983). *J. Appl. Cryst.* **16**, 204–211.
MOXON, J. R. L. & RENSHAW, A. R. (1990). *J. Phys. Condens. Matter*, **2**, 6807–6836.
NYE, J. F. (1979). *Physical Properties of Crystals.* Oxford Univ. Press.
TESSMAN, J. R., KHAN, A. H. & SHOCKLEY, W. (1954). *Phys. Rev.* **92**, 890–895.
THOMAS, P. A., TEBBUTT, I. J. & GLAZER, A. M. (1991). *J. Appl. Cryst.* In the press.
VISHNEVSKII, V. N., ROMANYUK, N. A. & STEFANSKII, I. V. (1965). *Opt. Spectrosc.* **18**, 468–469.
VISHNEVSKII, V. N. & STEFANSKII, I. V. (1966). *Opt. Spectrosc.* **20**, 195–196.
WINCHELL, A. N. & WINCHELL, H. (1964). *The Microscopical Characters of Artificial Inorganic Solid Substances.* New York: Academic Press.

Acta Cryst. (1992). B**48**, 21–30

A Position-Space Model for Superconductivity in $YBa_2Cu_3O_{7-x}$

BY R. H. BUTTNER, E. N. MASLEN AND N. SPADACCINI

Department of Physics, University of Western Australia, Nedlands, Australia 6009

(*Received* 13 *January* 1989; *accepted* 2 *September* 1991)

Abstract

$M_r = 666.2$, orthorhombic, *Pmmm*, $Z = 1$, λ(Mo $K\alpha$) = 0.71069 Å, $F(000) = 294$, $T = 298$ K. Data set (1): $a = 3.847$ (4), $b = 3.875$ (4), $c = 11.70$ (1) Å, $V = 174.44$ (5) Å^3, $D_x = 6.341$ Mg m^{-3}, $\mu = 29.24$ mm^{-1}, $R = 0.055$, $wR = 0.041$ (O5 excluded), $R = 0.053$, $wR = 0.037$ (O5 included) for 1132 unique reflections. Data set (2): $a = 3.842$ (1), $b = 3.886$ (1), $c = 11.690$ (4) Å, $V = 174.55$ (2) Å^3, $D_x = 6.338$ Mg m^{-3}, $\mu = 29.32$ mm^{-1}, $R = 0.046$, $wR = 0.041$ (O5 excluded), $R = 0.046$, $wR = 0.040$ (O5 included) for 1134 unique reflections. The structure is disordered with an O4 site occupancy of 0.54 (2) for data set (1) and 0.64 (2) for data set (2). The $\Delta\rho$ maps for the structure have characteristics consistent with those of cubic perovskites, but modified as expected for the distorted structure. For both experiments, the nature of the depletion of electron density near Cu1 is as expected for a cooperative Jahn–Teller-distorted Cu system. Its radial dependence is consistent with depletion of paired spins along the Cu1—O1 bond, and of unpaired spins along the Cu1—O5—Cu1 vector. $\Delta\rho$ associated with Cu2 is strikingly dissimilar to that near Cu1. The density near the O5 site is not accounted for adequately by a disordered model since the mean-square amplitudes of vibration with refined occupation determined by least squares are non-physical. The main characteristics of $\Delta\rho$ in the (001) plane containing the O5 site could be inferred from the $\Delta\rho$ topology of the archetypal $KCuF_3$ structure which has been accurately determined. The mechanism proposed for coupling the redistributed electron density with the vibrational motion of Cu1 in the [100] direction involves modulation by that motion of the antiferromagnetic exchange between adjacent Cu1 atoms.

Introduction

In the standard BCS theory of superconductivity, electron pairs with momentum/spin $\hbar\mathbf{k}^{\uparrow}$, $-\hbar\mathbf{k}^{\downarrow}$ are coupled to hole pairs with momentum $\hbar\mathbf{k}'^{\uparrow}$, $-\hbar\mathbf{k}'^{\downarrow}$ by phonon interactions which lower the total energy (Rickayzen, 1965). This is usually represented in **k** space. Most high-T_c superconducting compounds reported to date contain Cu and have distorted perovskite structures. As BCS theory gives a satisfactory description of type I and type II superconductors, **k**-space representations are preferred in most theoretical studies of the high-T_c oxide superconductors. However, as the coherence length in the oxide system is closer to the cell size, position-space treatments may have some advantages in explaining the phenomenon.

It is probable that the electron density has characteristics common to the perovskite series which are relevant to the superconducting properties of particular members. The simplest distorted member of that structural class, $KCuF_3$, is not superconducting, but its electron density can be determined with high precision because it contains no atoms with high atomic number. Accurate analyses of $KCuF_3$ by Spadaccini (1988), Tanaka, Konishi & Marumo (1979), Tanaka & Marumo (1982) and Buttner, Maslen & Spadaccini (1990), provide the information necessary for a detailed comparison with superconducting perovskites.

Johnson, McHenry, Counterman, Collins, Donovan, O'Handley & Kalonji (1988) have proposed a

0108-7681/92/010021-10$03.00

position-space model for superconductivity in La_2CuO_4 and $YBa_2Cu_3O_{7-x}$. The theory involves O(p)—O(p) π-bonding/Cu(d)—O(p) π-antibonding orbitals at the Fermi energy level with dynamic and pseudo Jahn–Teller coupling. The predicted T_c for orthorhombic $YBa_2Cu_3O_{7-x}$ ranges from 90 to 139.2 K depending on correlation distances and the coherence lengths which are of the order of 17–22 Å. T_c values predicted for other materials are also tabulated in that paper. However for $YBa_2Cu_3O_{7-x}$ at least, higher T_c values have been reported. For example, a T_c of 159 K was achieved by temperature cycling (Bhargava, Herko & Osborne, 1987). The TEM analysis of Sarikaya & Stern (1988) supports that observation, reporting variations of $\Delta a/a$ $[=2(b-a)/(a+b)]$ in the range of 0–4% over distances of 1000 Å. The high T_c suggested by Sarikaya & Stern (1988) would also imply reduced coherence lengths, the lower limits being the cell dimensions. The inference is a T_c limit for the material of 220 K obtained by maximizing $\Delta a/a$, and therefore minimizing O4–O5 disorder, as discussed by those authors.

X-ray diffraction results are not fully consistent with this hypothesis. The accurate single-crystal analysis of Paulus, Hoechst, Brodt, Fuess, Assmus & Kowalewski (1988) reports a small $\Delta a/a$ of 1.49%. There is a tendency for the material to disorder over the O4–O5 sites (see Figs. 1*a* and 1*b*), but the degree of disorder derived in that study is low. If the hypothesis had been correct, a larger $\Delta a/a$ value should have resulted.

It is difficult to achieve high accuracy in single-crystal analyses for $YBa_2Cu_3O_{7-x}$ for reasons described by Hazen (1988) but the reliability indices achieved are such that the $\Delta\rho$ maps should be qualitatively correct. Furthermore the structure is closely related to the more ideal perovskites and the latter, when studied accurately, followed trends characteristic of the series generally. The degree of consistency with those trends provides a test of the reliability of the electron density determined for a high-T_c distorted perovskite structure.

Crystal preparation of $YBa_2Cu_3O_{7-x}$

'Recipes' for producing single crystals of $YBa_2Cu_3O_{7-x}$ abound in the current literature. Even so, few accurate analyses are reported due to the difficulty of preparing high-quality single crystals. Several techniques for growing specimens were investigated. The main problem encountered was containment of the partial melt of the component oxides. Solid-state reactions producing powder samples present few difficulties because there is very little contamination. The use of excess Cu and Ba oxides as a flux for crystal growth, as reported by Dinger, Worthington, Gallagher & Sandstrom (1987), greatly increases the probability of contamination since extensive melting occurs. Table 1 lists crucible materials used in various attempts to produce 'ideally imperfect' specimens suitable for electron density studies.

Table 1. *Crucible materials investigated for* $YBa_2Cu_3O_{7-x}$ *crystal preparation*

Material	Reference	Result
(1) Y_2O_3 (pellet)	(*a*)	Extensive absorption of melt by pellet
(2) Pt-lined Al_2O_3	(*b*)	Corrosion of foil with some crystallization
(3) Ta_2O_5 (pellet)	After (*c*)	Extensive absorption of melt by pellet, well faceted Y_2BaCuO_5 crystals
(4) ZrO_2 (pellet)		Extensive absorption of melt by pellet, some Y_2BaCuO_5 crystals
(5) Zirconia (crucible)	(*d*)	Extensive absorption of melt by crucible, no crystallization
(6) Cu (crucible)	Present experiment	N_2 atmosphere during heating, O_2 flow below 923 K, melt creeps and reacts with Cu
(7) CuO (pellet)	Present experiment	Suitable method
(8) Al_2O_3	Present experiment	Suitable, but with some contamination

References: (*a*) Takei, Takeya, Iye, Tamegai & Sakai (1987). (*b*) Darlington, O'Connor & Hollin (1988). (*c*) Yurek, Van der Sande, Wang, Rudman, Zhang & Matthiesen (1987). (*d*) Menken & Menovsky (1988).

Initially crystals were grown using stoichiometric quantities of BaO_2 (or Ba_2CO_3), CuO and Y_2O_3 ground and pressed into a pellet, heated at 1175 K for 24 h before cooling by approximately 20 K h^{-1} to 543 K. The pellet sizes were then varied over the range 0.5 to 1.5 cm in height and diameter. In most trials BaO_2 was preferred to Ba_2CO_3 – a procedure used successfully by Calastani & Rizzoli (1987) for crystallization of $YBa_2Cu_3O_{7-x}$. Of the different peak-heating temperatures investigated the most suitable was 1345 K.

An SEM EDAX analysis of crystals grown using an Al_2O_3 crucible indicated contamination of the partial melt, concentrated in regions of direct contact with the crucible. There was no indication of Al in crystals formed in small cavities within the pellet. One such crystal from a batch not treated with oxygen during the final cooling process was used for data collection. A more satisfactory approach to avoiding contamination was placing pressed material on a CuO substrate which also provides excess CuO as a flux. To promote oxygen absorption and decrease the 'x' value, O_2 gas was passed into the oven between 923 to 573 K, *i.e.* from above to below the oxygen-absorption range reported by Ono & Tanaka (1987). A second set of data was measured using a crystal prepared by this latter method.

Experimental

The first specimen selected for data collection was an approximate trapezium-based prism having two {010}, two {001} and two {110} faces and volume

Table 2. *Experimental and refinement data*

	Data set (1)	Data set (2)
Diffractometer	Syntex $P2_1$	Syntex $P2_1$
Monochromator	Graphite	Graphite
Scan type	$\omega/2\theta$	$\omega/2\theta$
Scan speed (° min^{-1})	8.37	6.51
Peak scan width ($a + b\tan\theta$)	1.7; 0.7	2.7; 0.7
Max. 2θ (°)	100	100
Max. intensity variation of standards (%)		
200 020 006	3.3	
± 060 ± 005		1.0
Number of reflections measured	6399	8646
Transmission range	0.16; 0.33	0.14; 0.45
R_{int} (before and after absorption)	0.095; 0.057	0.031; 0.029
Number of independent reflections	1132	1134
R (O5 excluded)	0.055	0.046
R (O5 included)	0.053	0.046
wR (O5 excluded)	0.041	0.041
wR (O5 included)	0.037	0.040
S (O5 excluded)	2.56 (5)	5.6 (1)
S (O5 included)	2.34 (5)	5.4 (1)
Weights	$1/\sigma^2(F_o)$	$1/\sigma^2(F_o)$
Final max. shift/e.s.d. (O5 excluded)	0.00018	0.00027
Final max. shift/e.s.d. (O5 included)	0.00012	0.00189
Max. height in final difference Fourier (O5 excluded) (e Å^{-3})	13.2 (5)	10.1 (3)
Max. height in final difference Fourier (O5 included) (e Å^{-3})	10.9 (5)	10.2 (3)
Min. height in final difference Fourier (O5 excluded) (e Å^{-3})	−9.6 (5)	−8.6 (3)
Min. height in final difference Fourier (O5 included) (e Å^{-3})	−9.7 (5)	8.6 (3)
Min. extinction y	0.93	0.89

3.74×10^{-4} mm^3, damage to some faces having occurred in extracting the crystal from the bulk. The well faceted specimen cleaved from a larger plate-like crystal for data set 2 was a trapezium-based prism with one {001}, one {101}, two {100} and two {010} faces of approximate volume 2.06×10^{-4} mm^3.

All data were measured on a Syntex $P2_1$ diffractometer using Mo $K\alpha$ radiation ($\lambda = 0.71069$ Å). Experimental details are set out in Table 2. Data set (1) consisted of approximately two-thirds of a sphere of reflections, $(\sin\theta/\lambda)_{max} = 1.0803$ Å^{-1}, $-8 \le h \le 3$, $-8 \le k \le 8$, $-25 \le l \le 25$. Data set (2) spanned a full sphere $-8 \le h \le 8$, $-8 \le k \le 8$, $-25 \le l \le 25$. Absorption corrected analytically (Alcock, 1974), Lorentz and polarization corrections applied. Full-matrix least-squares refinement based on $|F|$. All measured structure factors included in refinements.

The reference state for all structure-factor calculations was the independent atom model. Atomic scattering factors from Cromer & Mann (1968) and anomalous-dispersion corrections from Cromer & Liberman (1970). Anisotropic thermal parameters and isotropic extinction parameter (Larson, 1970) refined. Details of refinements, including and excluding O5, are listed in Table 2. All calculations utilized the *XTAL* system of crystallographic programs (Hall & Stewart, 1987, 1988, 1989). The structural parameters are in Table 3* and the structure is depicted in Fig. 1.

* Lists of structure factors and anisotropic thermal parameters, and figures for data set (2) have been deposited with the British Library Document Supply Centre as Supplementary Publication No. SUP 54566 (42 pp.). Copies may be obtained through The Technical Editor, International Union of Crystallography, 5 Abbey Square, Chester CH1 2HU, England.

Table 3. *Anisotropic thermal parameters ($U \times 10^4$ Å^2) and atomic fractional coordinates for data sets (1) and (2)*

Results for the second analysis follow those of the first for each table entry.

$$T = \exp[-2\pi^2(h^2a^{*2}U_{11} + k^2b^{*2}U_{22} + l^2c^{*2}U_{33})].$$

	x	y	z	U_{11}	U_{22}	U_{33}
O5 excluded						
Ba	0.5	0.5	0.18598 (3)	135 (2)	110 (2)	76 (1)
	0.5	0.5	0.18536 (4)	129 (2)	84 (2)	81 (2)
Y	0.5	0.5	0.5	81 (4)	69 (3)	52 (3)
	0.5	0.5	0.5	76 (4)	60 (3)	56 (4)
Cu1	0.0	0.0	0.0	169 (7)	132 (5)	59 (4)
	0.0	0.0	0.0	155 (6)	139 (5)	64 (5)
Cu2	0.0	0.0	0.35642 (7)	68 (4)	63 (3)	81 (3)
	0.0	0.0	0.35619 (8)	63 (3)	46 (3)	89 (4)
O1	0.0	0.0	0.1576 (5)	221 (31)	222 (25)	98 (17)
	0.0	0.0	0.1581 (5)	248 (31)	189 (23)	100 (21)
O2	0.5	0.0	0.3789 (4)	80 (23)	129 (18)	91 (16)
	0.5	0.0	0.3788 (4)	89 (21)	85 (18)	110 (20)
O3	0.0	0.5	0.3785 (4)	99 (23)	73 (16)	88 (15)
	0.0	0.5	0.3776 (4)	132 (23)	60 (17)	96 (19)
O4	0.0	0.5	0.0	243 (88)	69 (47)	114 (50)
	0.0	0.5	0.0	368 (90)	110 (51)	108 (54)
Population O4: data set (1) = 0.54 (2), data set (2) = 0.64 (2)						
O5 included						
Ba	0.5	0.5	0.18598 (3)	136 (2)	111 (2)	77 (1)
	0.5	0.5	0.18534 (4)	129 (2)	85 (2)	83 (2)
Y	0.5	0.5	0.5	82 (4)	69 (3)	53 (3)
	0.5	0.5	0.5	77 (4)	62 (3)	56 (4)
Cu1	0.0	0.0	0.0	170 (6)	134 (5)	61 (4)
	0.0	0.0	0.0	158 (6)	140 (5)	65 (5)
Cu2	0.0	0.0	0.35645 (6)	68 (3)	64 (2)	81 (3)
	0.0	0.0	0.35619 (8)	63 (3)	47 (3)	90 (4)
O1	0.0	0.0	0.1577 (4)	212 (28)	221 (22)	96 (15)
	0.0	0.0	0.1580 (5)	243 (29)	187 (22)	99 (20)
O2	0.5	0.0	0.3782 (4)	87 (21)	128 (17)	88 (14)
	0.5	0.0	0.3786 (4)	101 (21)	95 (18)	105 (19)
O3	0.0	0.5	0.3786 (4)	105 (23)	75 (15)	88 (14)
	0.0	0.5	0.3775 (4)	136 (23)	64 (17)	93 (19)
O4	0.0	0.5	0.0	217 (77)	62 (42)	121 (50)
	0.0	0.5	0.0	322 (80)	101 (48)	122 (54)
O5	0.5	0.0	0.0	26 (120)	540 (218)	82 (92)
				U_{iso}		
O5	0.5	0.0	0.0	11 (54)		

Population O4: data set (1) = 0.53 (2), data set (2) = 0.64 (2)
Population O5: data set (1) = 0.26 (2), data set (2) = 0.14 (2)

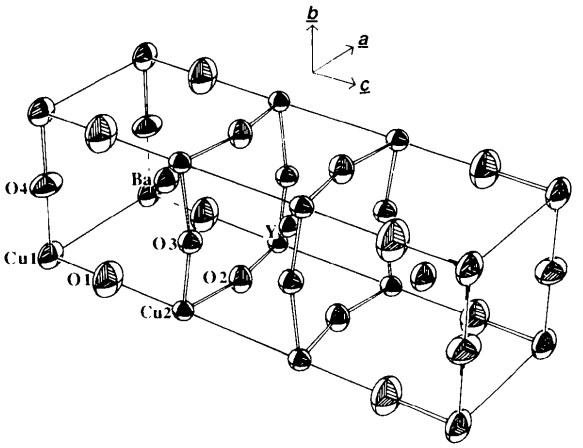

Fig. 1. $YBa_2Cu_3O_{7-x}$ cell structure with vibrational ellipsoids at the 95% probability level for data set (1), excluding atom O5.

The changes in parameters when O5 is introduced into the refinement are small, but the thermal parameters of O5 are unrealistic. For data set (1) U_{11} for O5 is half the value of any other mean-square thermal amplitude for the structure, whereas U_{22} is more than twice any other value. For data set (2) the thermal parameters for O5 would not refine anisotropically, and to achieve convergence with isotropic motion the population was first refined independently and then fixed. It is notable that the single-crystal X-ray analysis of Paulus *et al.* (1988), for which the population is similar, reports only an isotropic thermal parameter for O5. In the neutron single-crystal study of Hoydoo, McMullen, Axe, Cox, Lui, Crabtree & Lam (1987) the O5 population, 0.1 (1), is low and is in agreement with the neutron powder studies of Capponi, Chaillout, Hewat, Lejay, Marezio, Nguyen, Raveau, Soubeyroux, Tholence & Tournier (1987). The probable conclusion is that, while the site is partly occupied, the refined occupancy is exaggerated by redistribution of electron density due to chemical bonding.

The thermal parameters for cations in both refinements follow the trend $U_{11} > U_{22} > U_{33}$, except for Cu2 where $U_{22} < U_{33}$, as expected from its stereochemistry. The significantly lower U_{22} for Cu2 and Ba in the second refinement might be related to the contraction of the *a* and *c* axes for data set (2), but the increased U_{33} for all cations in that refinement cannot reasonably be ascribed to cell-length variations. The small changes observed may be influenced by the decrease in the O5 population, which would affect the motion of Ba directly and those of most other atoms indirectly. The larger e.s.d.'s of the thermal parameters for the O atoms make it difficult to identify any trend, except for the close agreement between the refinements. Significantly, the U_{11} value of Cu1 is the largest thermal-tensor component for any cation in both analyses. The result is not unexpected in view of the openness of the structure in the *a* direction, and the vibrational amplitudes of 0.13 (2) and 0.12 (2) Å for data sets (1) and (2) respectively are obviously important in considering transport phenomena.

Structural geometry

Table 4 lists the main interaction distances in the structure. There are differences between the data sets related to the contraction and expansion of the *a* and *b* axes. The largest change is for the Cu2—O1 contact, which actually exceeds that expected from the contraction of the *c* axis. In the repositioning associated with the population decrease of the O5 site, the Ba—O1 vector length is more accurately maintained.

An isolated Cu atom in a stationary d^9 state could be situated in a perfectly octahedral ligand field. For an unpaired d^9 electron full octahedral geometry is unstable against small perturbations, because of the degeneracy of the d^9 state, as predicted by the Jahn–Teller (1937) theorem. That theorem does not specify the type of distortion. For Cu the common distortion to D_{4h} symmetry has one axis of the octahedron elongated and the other two contracted. The ideal Cu1 geometry is approximately of this type, except

Table 4. *Selected interaction vector lengths* (Å) *and angles* (°) *for* $YBa_2Cu_3O_{7-x}$ *and comparative lengths* (Å) *for data set* (1) *with those found in other compounds*

Data set (1)/data set (2) arranged as in Table 3 (superscript indicates multiplicity).

	Coordination	Interaction length		Angle	
Ba	10	Ba—O1	2.750 (2)[8]	O1—Ba—O1	88.76 (8); 89.57 (9)
			2.7510 (9)[8]		88.87 (3); 89.59 (3)
		Ba—O4	2.905 (2)[4]	O4—Ba—O4	82.95 (9)
			2.8958 (7)[4]		83.12 (3)
		Ba—O3	2.962 (4)[4]	O3—Ba—O3	81.0 (1)
			2.957 (4)[4]		81.0 (1)
		Ba—O2	2.975 (4)[4]	O2—Ba—O2	81.3 (1)
			2.982 (4)[4]		81.3 (1)
Cu1	4	Cu1—O1	1.844 (6)[8]		
			1.848 (6)[8]		
		Cu1—O4	1.938 (2)[8]		
			1.9431 (6)[8]		
Cu2	5	Cu2—O2	1.942 (2)[8]	O2—Cu2—O2	164.4 (2)
			1.9393 (9)[8]		164.3 (2)
		Cu2—O3	1.955 (2)[8]	O3—Cu2—O3	164.8 (2)
			1.9592 (9)[8]		165.3 (2)
		Cu2—O1	2.327 (6)[8]		
			2.315 (6)[8]		
Y	8	Y—O3	2.392 (3)[4]	O3—Y—O3	107.1 (2)
			2.395 (3)[4]		106.6 (1)
		Y—O2	2.401 (3)[4]	O2—Y—O2	107.6 (2)
			2.405 (3)[4]		107.8 (1)

M—*M* contacts (< 4.0 Å)

	Ba		Y		Cu1	Cu2
Ba	3.847 (4)	3.875 (4)	3.674 (4)		3.491 (2)	3.381 (2)
	3.842 (1)	3.886 (1)	3.678 (1)		3.4873 (7)	3.3844 (8)
Y			3.847 (4)	3.875 (4)		3.206 (2)
			3.842 (1)	3.886 (1)		3.2082 (7)
Cu2						3.360 (4)
						3.362 (2)

Cu—Ba—Cu angles

Cu1—Ba—Cu1	66.87 (7)[4]	67.41 (7)[4]	Cu2—Ba—Cu2	69.35 (7)[4] 69.92 (7)[4]
	66.86 (2)[4]	67.72 (2)[4]		69.17 (2)[4] 70.08 (2)[4]

	Vector	length	Structure	Comparative	lengths	Ref.
Cu1	Cu1—O4	1.938 (2)	$KCuF_3$	Cu—F	F1 1.9622 (2)	(*a*)
	Cu1—O1	1.844 (6)		(short)	F2 1.8888 (4)	
	{Cu1—O5	1.924 (2)}		(long)	F2 2.2527 (4)	
Cu1	Cu1—Cu1	3.847 (4)				
Cu2	Cu2—O1	2.327 (6)	CuO	Cu—O	1.9608 (13)	(*b*)
	Cu2—O2	1.942 (2)			1.9509 (26)	
	Cu2—O3	1.955 (2)			2.7840 (37)	
			Cu_2O	Cu—O	1.848	(*c*)
	Cu2—Cu2	3.360 (4)	CuO	Cu—Cu	2.9005 (3)	(*b*)
					3.0830 (4)	
					3.1734 (4)	
					3.7484 (4)	
			Cu_2O	Cu—Cu	3.017	(*c*)
			Cu	Cu—Cu	2.5560	(*d*)
Y	Y—O2	2.401 (3)	Y_2O_3	Y1—O	2.2475 (9)	(*e*)
	Y—O3	2.392 (3)		Y2—O	2.2619 (12)	
					2.2796 (22)	
					2.3448 (14)	
Ba	Ba—O1	2.750 (2)	BaO	Ba—O	2.762	(*f*)
	Ba—O2	2.975 (4)	BaO_2	Ba—O	2.68	(*g*)
	Ba—O3	2.962 (4)			2.79	
	Ba—O4	2.905 (4)				

References: (*a*) Buttner *et al.* (1990). (*b*) Åsbrink & Norrby (1970). (*c*) Restori & Schwarzenbach (1986). (*d*) National Bureau of Standards (1953). (*e*) Paton & Maslen (1965). (*f*) Wyckoff (1963). (*g*) Abrahams & Kalnajs (1954).

that Cu1—O1 is 0.094 (6) Å [0.095 (6) Å for data set (2)] shorter than Cu1—O4, and the oxygen O5, along the vector orthogonal to the O1—Cu1—O4 plane, *i.e.* the direction of elongation, is missing.

Table 4 also lists selected interaction vectors from data set (1) involving the cations Cu1, Cu2, Ba and Y with corresponding interaction lengths in related compounds included for comparison. The Cu1 interaction lengths resemble the equivalent $KCuF_3$ values closely, except for the elongated vector. If the O1, O4 and O5 sites are occupied simultaneously there is no elongated axis. On the premise that Cu1—O1 and Cu1—O4 are Jahn–Teller-contracted, the only possible elongated Jahn–Teller vector is Cu1—Cu1 along the *a* axis. This explanation for the Cu1 geometry involves a change from a Cu-anion to Cu-cation interaction. It is difficult to predict Cu—*X* bond lengths accurately given the widely varying degrees of anisotropy observed in Cu bonding, but the minimum value of 3.72 Å for the *a* axis reported by Sarikaya & Stern (1988) is broadly consistent with the long Cu—Cu distance observed for the similar copper–oxygen environment in CuO. Ordering of the basal plane oxygen O4 in $YBa_2Cu_3O_{7-x}$ is obviously difficult, as indicated by the disorder and by the high thermal motion in that region.

The structural geometry involving Cu2 differs markedly from the ideal. The Cu2—O2 and Cu2—O3 bonds are displaced from the ideal octahedron by approximately 7.7° toward the $z = \frac{1}{2}$ plane. The extended Cu2—O1 interaction length is 2.327 (6) Å [2.315 (6) Å for data set (2)]. The opposite O site is unoccupied. The nearest symmetry-related Cu2 atom is 3.360 (4) Å [3.362 (2) Å for data set (2)] away. This distance is longer than the Cu—Cu contact in Cu metal (2.5560 Å). As these positions are not those expected for a Jahn–Teller-distorted D_{4h} system, a detailed analysis of the environment is appropriate.

The coordination geometry for Cu2 resembles that for the Cu atom in Y_2BaCuO_5 (Buttner, 1990) *i.e.* it is not coplanar with the four O ligands and the Cu2—O1 contact is extended. The Cu2 interaction lengths are also similar to those for Cu in CuO (Åsbrink & Norrby, 1970) except for the extended Cu2—O1 vector. The Y coordination number of eight in $YBa_2Cu_3O_{7-x}$ is larger than the value of six in Y_2O_3 (Paton & Maslen, 1965), explaining the small increase in Y—O lengths. Presumably the coordination of Cu2 with another Cu atom in place of O is due to the dominance of Y—O bonding in the middle part of the cell. The occasional observation of an O atom between the two Cu2 atoms, generating a layer fault in imperfect structures (Ourmazd, Rentschler, Spence, O'Keeffe, Graham, Johnson & Rhodes, 1987) is consistent with this hypothesis.

The coordination of Ba with ten O atoms, resembling that in BaO_2, contrasts with only six in BaO. The only interaction length similar to those in either Ba oxide is Ba—O1. As O1 is also involved in the shortest Cu1—O distance, that atom is strongly bound. This does not support the in-plane breathing mode proposed by David, Harrison, Gunn, Moze, Soper, Day, Jorgensen, Hinks, Beno, Soderholm, Capone, Schuller, Segre, Zhang & Grace (1987). The low thermal motion for O1 and O4 in the directions corresponding to strong planar bonds is also inconsistent with such a mode. The extended lengths for the other Ba vectors are expected in view of the high coordination number of the Ba atom, and the small values for some O—Ba—O angles involving O1, O2 and O3. The corresponding O—Y—O angles are enlarged because Y is smaller than Ba. The Ba—O bonds extend to relieve exchange repulsion between the atoms involved in small O—Ba—O angles.

Difference density

Owing to the high atomic numbers of Ba and Y and the uncertain quality of the crystals, it was necessary to check the reliability of the difference maps before attributing major features to movements of electron density due to bonding. An internal check is provided by the consistency of the density in chemically similar parts of the structure. Accurate difference densities for more ideal perovskite structures contain characteristic features (Maslen & Spadaccini, 1989) which can be used to test the reliability of the difference maps in the more difficult case of $YBa_2Cu_3O_{7-x}$. $\Delta\rho$ sections for the first analysis are plotted in Figs. 2 to 5. The contour interval for mapping is 2 e Å^{-3} with ± 1 e Å^{-3} included to display finer detail. The corresponding maps for data set (2) are deposited with the structure factors.*

Figs. 2(*a*) and 2(*b*) depict chemically similar parts of the (100) and (010) sections containing Cu2, with O3 and O2 respectively, for data set (1). Noting $\sigma(\Delta\rho)$ of 0.5 e Å^{-3} determined by the method of Cruickshank (1949), the agreement to within one contour is as close as is expected for chemically equivalent moities. However, there is little correspondence between the density in regions closer to O4 and O5, as shown in Figs. 3(*a*) and 3(*b*). This is confirmed in the deposited maps for the same regions for data set (2).

Maslen & Spadaccini (1989) describe a characteristic depletion of electrons at the structural cavity for perovskites containing six-coordinated transition metals with nearly filled 3*d* subshells. That is reflected in the depletion of the electron density at the points 'X' in Fig. 2, and occurs at 'X' marked in

* See deposition footnote.

Fig. 4, the (001) plane with $z = 0.3564$. Topological characteristics of $\Delta\rho$ in Fig. 4 closely resemble those for the corresponding (001) plane in the cubic $KZnF_3$ perovskite (Buttner & Maslen, 1988).

Although the topology is not completely equivalent for the two data sets, there is very good agreement for chemically related sections within each experiment. Where the electron densities for the two samples differ, the density may be related to the different degree of O4 ordering, which alters the cell dimensions for the two samples.

Both the internal consistency of the maps and the close relationship of characteristic features to those in other perovskite compounds indicate that the difference density maps contain chemically significant information. This is reinforced when the relationship of the features to the small structural differences between the two analyses is studied in greater detail. The O—O vectors in Figs. 2(*a*) and 2(*b*) are reduced in length by displacement of O2 and O3 towards the plane with $z = 0.5$. The exchange depletion of the electron density extends along the foreshortened O—O contacts in a manner similar to that along the shortest F—F vectors in the $KCuF_3$ structure (Buttner *et al.*, 1990). Further agreement with $KCuF_3$ is displayed in Figs. 3(*a*) and 3(*b*), where six minima within 0.8 Å of the Cu1 nucleus closely resemble those near the Cu atom in $KCuF_3$. The depletion furthermost from the nuclear position for the short Cu—O contact is slightly more diffuse for the second data set. The $\Delta\rho$ topography is also consistent with that for Cu in $(NH_4)_2Cu(SO_4)_2.6H_2O$ (Maslen, Watson & Moore, 1988). However the polarization for $YBa_2Cu_3O_{7-x}$, as indicated by the depth of the minima, is markedly stronger.

The topography of the difference density near Cu2 differs from that near Cu1, *i.e.* from the polarization expected from an ideal d^9 configuration, the discrep-

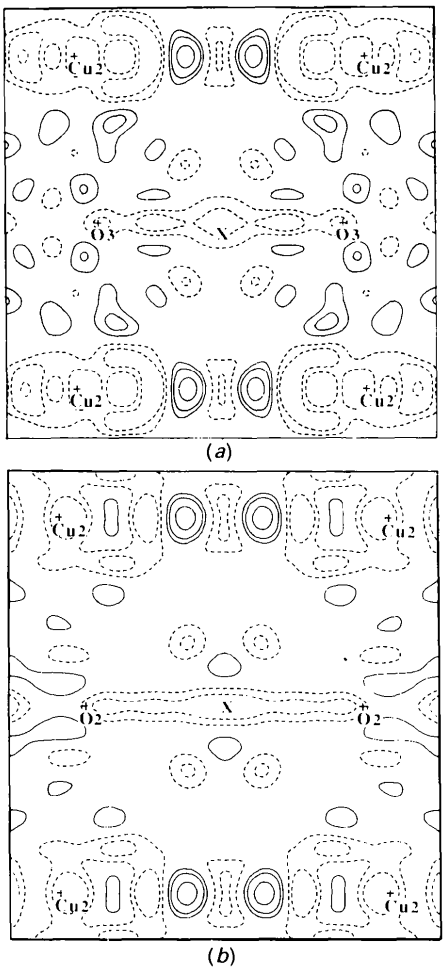

Fig. 2. Data set (1) $\Delta\rho$ for $YBa_2Cu_3O_{7-x}$ in (*a*) the (100) plane, map borders 5.0 by 5.0 Å and (*b*) the (010) plane, map borders 4.8 by 4.4 Å. Contour intervals 2 e Å^{-3} with −1, 1 e Å^{-3} included, positive, negative contours – solid, short dashes respectively.

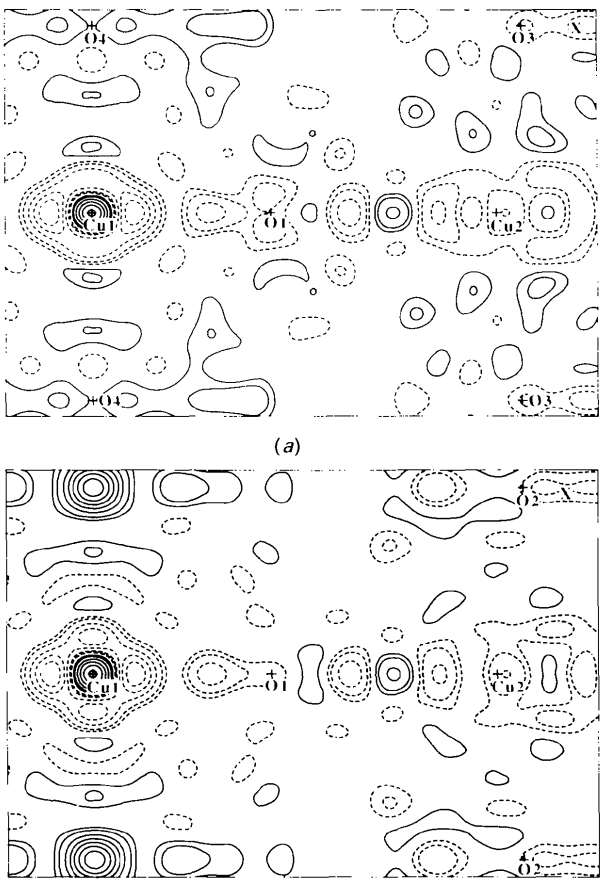

Fig. 3. Data set (1) $\Delta\rho$ for $YBa_2Cu_3O_{7-x}$ in (*a*) the (100) plane and (*b*) the (010) plane. Map borders 6.1 by 4.2 Å. Contouring as in Fig. 2.

ancy being especially pronounced for data set (1). In both analyses, there is a local minimum very close to the Cu2 nucleus, with additional polarization along the Cu2—O2 and Cu2—O3 vectors. The more significant features lie along the shorter Cu2—Cu2 vectors within Figs. 2(*a*) and 2(*b*). Along that vector in Fig. 2(*a*), the $\Delta\rho$ value is 0.8 e Å^{-3} at 0.6 Å from Cu2, -3.9 e Å^{-3} at 1.0 Å, rising to 5.0 e Å^{-3} at 1.3 Å, before falling to a minimum of -2.1 e Å^{-3} at the midpoint, in very close agreement with the corresponding sequence in Fig. 2(*b*). The equivalent heights are 3.0, 1.0, 1.5 and -0.2 e Å^{-3} respectively for data set (2). The differences between values for the two data sets may be related to the thermal amplitudes of Cu2, U_{22} being significantly lower and U_{33} being higher for data set (2).

Electron density accumulates in the open region bisecting the *c*-axis Cu2—Cu2 vector. There is far less polarization of density along the Cu2—Cu2 vectors parallel to the *a* and *b* axes. The depletion of density near the Cu2 nucleus falls off rapidly along the line of the four Cu2—Y and Cu2—Ba vectors, of lengths 3.206 (2) and 3.381 (2) Å respectively. Maslen, Spadaccini, Watson & White (1986) have shown that the electron density is increased along the line of short contacts between Cu^{II} atoms and other cations. This may account for the non-ideal form of the difference density near Cu2 in this structure.

The $\Delta\rho$ topography characteristic of a Jahn–Teller-distorted D_{4h} system near Cu1 contrasts with that near Cu2. In analysis (1), the greatest depletion of density of -9.6 e Å^{-3} occurs 0.5 Å from the Cu1 along the short Cu1—O1 bond which compares to -7.6 e Å^{-3} at 0.4 Å in the *a*-axis direction. A similar inverse correlation of depth with distance occurs in $(NH_4)_2Cu(SO_4)_2.6H_2O$ (Maslen *et al.*, 1988) and at higher precision in $KCuF_3$ (Buttner *et al.*, 1990). As discussed in the latter study, one infers that for the short Cu—O1 vector, the 3*d* subshell is depleted of paired spin density and that closer to the Cu1 atom is depleted of 3*d* density with unpaired spin.

In $KCuF_3$ electron density is transferred from densely packed regions, indicated by low vibration along short bonds, to more open regions with longer bonds and larger motion. This principle applies equally well to the electron density for $YBa_2Cu_3O_{7-x}$, accounting for the accumulation of $\Delta\rho$ between Cu2 atoms noted above. Density also moves from the central part of the cell toward the less densely packed plane containing Cu1 and O4. In the model with no oxygen at the O5 position, $\Delta\rho$ peaks strongly at that site as shown in Fig. 5(*a*). The density is not well represented by the disordered O5 with refined populations of 0.26 (2) and 0.14 (2) for data sets (1) and (2) respectively, as is evident both from the refined *U* values and from the topography of $\Delta\rho$ with that atom included in the structure-factor

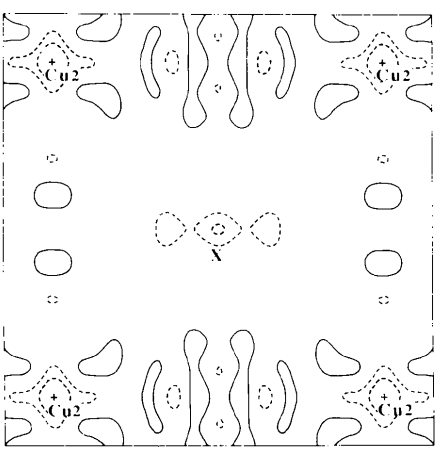

Fig. 4. Data set (1) $\Delta\rho$ for $YBa_2Cu_3O_{7-x}$ in the (001) plane with $z = 0.3564$. Map borders 5.0 by 5.0 Å, contouring as in Fig. 2.

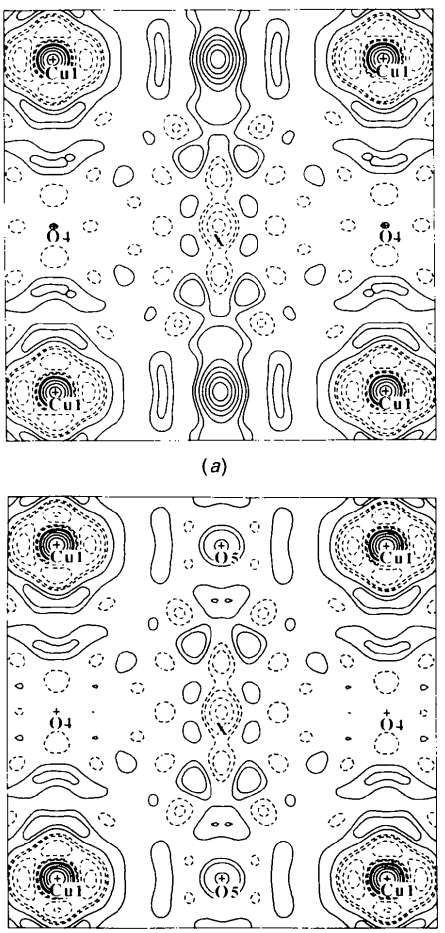

Fig. 5. Data set (1) $\Delta\rho$ for $YBa_2Cu_3O_{7-x}$ in the (001) plane with $z = 0$: (*a*) with O5 excluded from $|F_o|$ calculations and (*b*) with O5 included. Map borders 5.0 by 5.0 Å, contouring as in Fig. 2.

calculation, as shown in Fig. 5(*b*). One can reasonably infer that the character of $\Delta\rho$ for a fully ordered orthorhombic structure would be intermediate between Figs. 5(*a*) and 5(*b*). That indicates an energetically unfavourable concentration of electron density in a region of low electrostatic potential – an arrangement possible only if it is due to quantum mechanical interference (exchange) terms for paired electron spins.

The $\Delta\rho$ features near Cu1 in the $z = 0$ plane, Figs. 5(*a*) and 5(*b*), strongly resemble those near Cu in $KCuF_3$ displayed in Fig. 6. The radial dependence of the minima in the density nearer each Cu1 nucleus indicates the depletion of density to be spin polarized. The density as a whole can be viewed as transfer of electrons from the 3*d* state for neighbouring Cu atoms to distorted but overlapping 4*s* states maximizing at the bond centre, provided the 3*d* states for neighbouring Cu atoms have opposed spins, *i.e.* the system is antiferromagnetic.

The Jahn–Teller distortion of the electron density for the Cu1 atom is clearly an essential factor in determining the topography of the electron density in the Cu1–O4 plane shown in the figures above. Nevertheless the magnitudes of the features are larger than those observed in Cu compounds containing lighter atoms. One must therefore consider whether other characteristics of the structure contribute significantly to that polarization. Table 5 gives the set of atomic charges determined by the method of Hirshfeld (1977) for both data sets.

Given the similarity in vector lengths determined in both experiments, large changes are not expected, but measuring atomic charges accurately for materials containing atoms of high atomic number such as Y and Ba is difficult, to a degree which increases rapidly with extinction. The small number of reflections affected significantly by extinction are low-angle terms which predominantly reflect the transfer

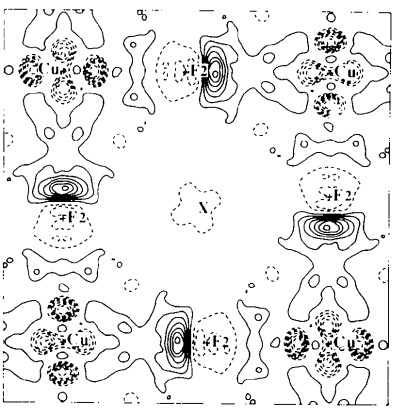

Fig. 6. $\Delta\rho$ for $KCuF_3$ in the (001) plane with $z = 0$. Map borders 6.0 by 6.0 Å, contour intervals 0.2 e Å $^{-3}$.

Table 5. *Atomic charges for data set* (1) *and data set* (2) *respectively*

	Charge (e)	Charge (e)
Ba	−0.6 (1)	1.24 (8)
Y	0.6 (1)	−0.96 (8)
Cu1	0.7 (1)	1.27 (8)
Cu2	0.6 (1)	−0.02 (8)
O1	0.9 (1)	−0.07 (6)
O2	−0.9 (1)	−0.48 (6)
O3	−0.5 (1)	−0.51 (6)
O4	−0.3 (1)	−0.61 (6)

of electrons between atoms in the structure. The effect of extinction is stronger for data set (2), which the reliability indices indicate to be of higher quality in other respects. Extinction limits the accuracy of the charges determined with that data set, especially for the heavier cations. Notwithstanding the lower formal standard deviations, the cation charges are expected to be less accurate for data set (2). For analysis (1), the topography of the depletion associated with the Ba is closer to that observed in Y_2BaCuO_5 by Buttner (1990) and Maslen (1989), also indicating $\Delta\rho$ for data set (1) to be more reliable in the vicinity of the heavy cations.

In analysis (1), the charges for the Y, Cu2, O2 and O3 atoms in the central third of the cell are consistent with atomic electronegativities. The result for Ba is counter-intuitive, as it appears to acquire a negative charge largely at the expense of O1. Owing to the large radius of the Ba atom the electrons accumulating near the vacant O5 site are largely assigned to the Ba atom in the charge partitioning for $YBa_2Cu_3O_{7-x}$. Electron density is moved from the short Cu1—O1 and Ba—O1 bonds and the close-packed region between Y and Ba into the space between adjacent Cu1—O1 bonds in the *a* direction at the top of the cell. Those regions are loosely packed, as indicated by the large vibrational amplitudes in that direction for Cu1 and O1. The accumulation of electron density there is consistent with the behaviour of $\Delta\rho$ in $KCuF_3$ (Buttner *et al.*, 1990). It is also consistent with five independent experiments on K_2PdCl_4 by Hester (1989). In the latter analyses electron density accumulates strongly at a structural hole. Hirshfeld partitioning consistently indicates a negative charge on the loosely packed K atom with a magnitude larger than that for Cl which is more tightly bound. The charges determined there are particularly sensitive to the algorithm for dividing electron density in the cavity between nearby anions and cations.

Model for superconductivity

As indicated above, theoretical calculations have been invoked to explain the high-T_c superconducting transition in $YBa_2Cu_3O_{7-x}$, with limited success.

Does the diffraction image of $\Delta\rho$ for $YBa_2Cu_3O_{7-x}$ provide significant further information? The topography of $\Delta\rho$ in the central region of the cell is consistent with that for more ideal perovskite structures, and that near Ba and Cu2 is consistent with the distribution in the non-superconducting Y_2BaCuO_5. Within 0.8 Å of Cu1, $\Delta\rho$ closely resembles that near the Cu atom in $KCuF_3$, for which density accumulates in a region along the Jahn–Teller-elongated axis as displayed in Fig. 6(*b*). Although an O analogue of F2 is missing in the ideal structure for $YBa_2Cu_3O_{7-x}$, electron density concentrates in the corresponding region midway between adjacent Cu atoms, especially near the midpoint of the shortest Cu1—Cu1 vector. The structure refinements indicate inconsistency of the structure factors with models which attribute that electron density at the O5 site solely to disordered oxygen. The density along the very weak bond may be partly described as transfer of unpaired electron density from the 3*d* subshell of each Cu atom to paired electron density near the bond centre, even though this is unfavourable energetically. This topography is characteristic of concentration of density by quantum mechanical interference terms due to overlap of electrons with paired spins. It requires antiferromagnetic ordering of spin in the structure.

As indicated in Table 3, the vibration amplitude for Cu1 parallel to (100) is the largest for any cation in the structure. As the *a*-axis Cu1—Cu1 vector expands and contracts the interference terms must change so that electrons flow towards and away from the bond. Among other things such a flow is necessary to create the restoring forces on the nuclei. The mode is extended in the *ab* plane, but is quite localized in the *c* direction, as is evident from the thermal amplitudes for Cu1 in Table 3. It is responsible for electron propagation which is large because of the size of the difference density features near the bond.

Thus $\Delta\rho$ is consistent with strong electron/phonon coupling, and charge movement results from the effect of nuclear vibrations, providing a mechanism for the resistance-free flow of electrons. Transition to the superconducting state is necessarily dependent on extended coupling of the motion of neighbouring Cu1 nuclei. As the electron density close to the Cu1 nuclei associated with the antiferromagnetism must change with internuclear distance, the antiferromagnetic exchange depletion close to the Cu1 nuclei is also modulated by the vibrational motion and would be partly responsible for the charge transfer. However, this antiferromagnetism does not have any special characteristic which justifies attributing superconductivity to it alone. Thus, the topography of $\Delta\rho$ and the vibration amplitudes for the structure are consistent with a vibrationally modulated exchange mechanism for the electron–hole pair motion necessary for high-T_c superconductivity.

Financial assistance from the Australian Research Council is acknowledged.

References

ABRAHAMS, S. C. & KALNAJS, J. (1954). *Acta Cryst.* **7**, 838–842.

ALCOCK, N. W. (1974). *Acta Cryst.* A**30**, 332–335.

ÅSBRINK, S. & NORRBY, L. J. (1970). *Acta Cryst.* B**26**, 8–15.

BHARGAVA, R. N., HERKO, S. P. & OSBORNE, W. N. (1987). *Phys. Rev. Lett.* **59**(13), 1468–1471.

BUTTNER, R. H. (1990). PhD Thesis, Univ. of Western Australia, Australia.

BUTTNER, R. H. & MASLEN, E. N. (1988). *Acta Cryst.* C**44**, 1707–1709.

BUTTNER, R. H., MASLEN, E. N. & SPADACCINI, N. (1990). *Acta Cryst.* B**46**, 131–138.

CALASTANI, G. & RIZZOLI, C. (1987). *Nature (London)*, **328**, 606–607.

CAPPONI, J. J., CHAILLOUT, C., HEWAT, A. W., LEJAY, P., MAREZIO, M., NGUYEN, N., RAVEAU, B., SOUBEYROUX, J., THOLENCE, J. L. & TOURNIER, R. (1987). *Europhys. Lett.* **3**(12), 1301–1307.

CROMER, D. T. & LIBERMAN, D. (1970). *J. Chem. Phys.* **53**, 1891–1898.

CROMER, D. T. & MANN, J. B. (1968). *Acta Cryst.* A**24**, 321–324.

CRUICKSHANK, D. W. J. (1949). *Acta Cryst.* A**24**, 65–84.

DARLINGTON, C. N. W., O'CONNOR, D. A. & HOLLIN, C. A. (1988). *J. Cryst. Growth*, **91**, 308–311.

DAVID, W. I. F., HARRISON, W. T. A., GUNN, J. M. F., MOZE, O., SOPER, O., DAY, P., JORGENSEN, J. D., HINKS, D. W., BENO, M. A., SODERHOLM, L., CAPONE, D. W., SCHULLER, I. K., SEGRE, C. U., ZHANG, K. & GRACE, J. D. (1987). *Nature (London)*, **327**, 310–312.

DINGER, T. R., WORTHINGTON, T. K., GALLAGHER, W. J. & SANDSTROM, R. L. (1987). *Phys. Rev. Lett.* **58**(25), 2687–2690.

HALL, S. R. & STEWART, J. M. (1987). Editors. *XTAL2.2 Users Manual*. Univs. of Western Australia, Australia, and Maryland, USA.

HALL, S. R. & STEWART, J. M. (1988). Editors. *XTAL2.4 Users Manual*. Univs. of Western Australia, Australia, and Maryland, USA.

HALL, S. R. & STEWART, J. M. (1989). Editors. *XTAL2.6 Users Manual*. Univs. of Western Australia, Australia, and Maryland, USA.

HAZEN, R. M. (1988). *Sci. Am.* **258**(6), 52–61.

HESTER, J. R. (1989). Private communication.

HIRSHFELD, F. L. (1977). *Isr. J. Chem.* **16**, 198–201.

HOYDOO, Y., MCMULLEN, R. K., AXE, J. D., COX, D. E., LUI, J. Z., CRABTREE, G. W. & LAM, D. J. (1987). *Solid State Commun.* **64**(5), 739–742.

JAHN, H. A. & TELLER, E. (1937). *Proc. R. Soc. London Ser. A*, **161**, 220–235.

JOHNSON, K. H., MCHENRY, M. E., COUNTERMAN, C., COLLINS, A., DONOVAN, M. M., O'HANDLEY, R. C. & KALONJI, G. (1988). *Physica*, C**153–155**, 1165–1166.

LARSON, A. C. (1970). *Crystallographic Computing*, edited by F. R. AHMED. Copenhagen: Munksgaard.

MASLEN, E. N. (1989). Unpublished confirmatory experiment.

MASLEN, E. N. & SPADACCINI, N. (1989). *Acta Cryst.* B**45**, 45–52.

MASLEN, E. N., SPADACCINI, N., WATSON, K. J. & WHITE, A. H. (1986). *Acta Cryst.* B**42**, 430–436.

MASLEN, E. N., WATSON, K. J. & MOORE, F. H. (1988). *Acta Cryst.* B**44**, 102–107.

MENKEN, M. J. V. & MENOVSKY, A. A. (1988). *J. Cryst. Growth*, **91**, 264–267.

NATIONAL BUREAU OF STANDARDS (1953). *Natl Bur. Stand. (US) Circ.* **539**(I), 15–16.
ONO, A. & TANAKA, T. (1987). *Jpn. J. Appl. Phys.* **26**(4), L825–L827.
OURMAZD, A., RENTSCHLER, J., SPENCE, J. C. H., O'KEEFFE, M., GRAHAM, G., JOHNSON, D. W. JR & RHODES, W. W. (1987). *Nature (London)*, **327**, 308–310.
PATON, M. G. & MASLEN, E. N. (1965). *Acta Cryst.* **19**, 307–310.
PAULUS, E. F., HOECHST, A. G., BRODT, K., FUESS, H., ASSMUS, W. & KOWALEWSKI, J. (1988). *Z. Kristallogr.* **185**, A4.
RESTORI, R. & SCHWARZENBACH, D. (1986). *Acta Cryst.* B**42**, 201–208.
RICKAYZEN, G. (1965). *Theory of Superconductivity*, Interscience Monographs and Texts in Physics and Astronomy, Vol. 14, edited by R. E. MARAHAK. New York: John Wiley.
SARIKAYA, M. & STERN, E. A. (1988). *Phys. Rev. B*, **37**(16), 9373–9381.
SPADACCINI, N. (1988). PhD Thesis, Univ. of Western Australia, Australia.
TAKEI, H., TAKEYA, H., IYE, Y., TAMEGAI, T. & SAKAI, F. (1987). *Jpn. J. Appl. Phys.* **26**(9), L1425–L1427.
TANAKA, K., KONISHI, M. & MARUMO, F. (1979). *Acta Cryst.* B**35**, 1303–1308.
TANAKA, K. & MARUMO, F. (1982). *Acta Cryst.* B**38**, 1422–1427.
WYCKOFF, W. G. (1963). *Crystal Structures*, 2nd ed., Vol 1. New York: Wiley–Interscience.
YUREK, G. J., VAN DER SANDE, J. B., WANG, W. X., RUDMAN, D. A., ZHANG, Y. & MATTHIESEN, M. M. (1987). *Metall. Trans.* A**18**, 1813–1817.

Acta Cryst. (1992). B**48**, 30–32

Cubic Structure of Chromium–Bromine Boracite at 298 and 113 K

BY M. YOSHIDA AND K. YVON

Laboratoire de Cristallographie, Université de Genève, 24 quai E. Ansermet, CH-1211 Genève 4, Switzerland

AND F. KUBEL AND H. SCHMID

Département de Chimie Minérale, Analytique et Appliquée, Université de Genève, 30 quai E. Ansermet, CH-1211 Genève 4, Switzerland

(*Received* 17 *June* 1991; *accepted* 10 *October* 1991)

Abstract

$Cr_3B_7O_{13}Br$, $M_r = 519.55$, cubic, $F\bar{4}3c$, $Z = 8$, $\lambda(Mo\ K\alpha) = 0.71073$ Å, $F(000) = 1968$. At 298 K: $a = 12.1524$ (1) Å, $V = 1794.68$ (3) Å^3, $D_x = 3.845$ Mg m^{-3}, $\mu = 8.533$ mm^{-1}, final $R = 0.020$ for 206 unique reflections with $I > 3\sigma(I)$; shortest interatomic distances (Å): Cr—O = 2.061 (2), Cr—Br = 3.03810 (3), B—O = 1.436 (3), O—O = 2.388 (2). At 113 K: $a = 12.1340$ (3) Å, $V = 1786.54$ (13) Å^3, $D_x = 3.863$ Mg m^{-3}, $\mu = 8.533$ mm^{-1}, final $R = 0.025$ for 281 unique reflections with $I > 3\sigma(I)$; shortest interatomic distances (Å): Cr—O = 2.057 (2), Cr—Br = 3.0335 (1), B—O = 1.436 (3), O—O = 2.390 (2). The planarity of the metal-centred CrO_4 groups does not differ significantly from that in other chromium-based cubic boracites and generally increases as the temperature is lowered.

Introduction

So far the cubic phases of seven boracites $M_3B_7O_{13}X$ (M = bivalent metal ion, X = halogen ion) based on 3*d* transition elements, M = Cr, Co, Ni, Cu, have been structurally characterized [for a review see Nelmes (1974); for later work see Monnier, Berset, Schmid & Yvon (1987), and references therein]. The metal ions in these structures are tightly bound to four nearly planar oxygen atoms and loosely bound to two apical halogen atoms. Most boracites (hereafter *M-X*) undergo structural phase transitions to non-cubic low-temperature modifications in which all (or part) of the metal ions strongly attract one of the halogen ligands. The known transition temperatures are situated between 60 K (Ni-I; Schmid, 1965) and 797 K (Cd-Cl; Schmid & Tippmann, 1978). With a view to investigating the factors responsible for this large temperature range we have decided to study cubic $Cr_3B_7O_{13}Br$ (hereafter Cr-Br). This compound together with Cr-I and Cu-I make up the exceptional and sole boracite compositions for which no structural transition to a non-cubic phase occurs down to very low temperature. This has been verified by observation in polarized light down to 10 K for Cr-Br and Cr-I (Schmid, 1965), reconfirmed for Cr-Br down to 9 K (Ye, 1991), and down to 15 K for Cu-I (Monnier *et al.*, 1987).

Experimental

Blue cube-shaped Cr-Br crystals were grown by the chemical vapour transport method (Schmid, 1965). Data collection: CAD-4 automatic four-circle diffractometer, graphite monochromator, liquid-

0108-7681/92/010030-03$03.00